THE ASTROPHYSICAL JOURNAL, 562:566–574, 2001 November 20

ELECTRON DENSITIES IN THE CORONAE OF THE SUN AND PROCYON FROM EXTREME-ULTRAVIOLET EMISSION LINE RATIOS IN Fe XI

D. J. PINFIELD,[1] F. P. KEENAN, AND M. MATHIOUDAKIS
Department of Pure and Applied Physics, The Queen's University of Belfast, Belfast, BT7 1NN, Northern Ireland
K. G. WIDING
Computational Physics Inc. and US Naval Research Laboratory, Washington, DC 20375-5000
P. T. GALLAGHER
Big Bear Solar Observatory, 40386 North Shore Lane, CA 92413-9672
G. P. GUPTA AND S. S. TAYAL
Department of Physics, Clark Atlanta University, Atlanta, GA 30314
R. J. THOMAS
Laboratory for Astronomy and Solar Physics, NASA Goddard Space Flight Center, Code 682, Greenbelt, MD 20771
AND
J. W. BROSIUS
Raytheon ITSS, 4400 Boulevard, Lanham, MD 20706
Received 2001 January 10; accepted 2001 July 24

ABSTRACT

New ***R***-matrix calculations of electron impact excitation rates for Fe XI are used to determine theoretical emission line ratios applicable to solar and stellar coronal observations. These are subsequently compared to solar spectra of the quiet Sun and an active region made by the Solar EUV Rocket Telescope and Spectrograph (SERTS-95), as well as *Skylab* observations of two flares. Line blending is identified, and electron densities of $10^{9.3}$, $10^{9.7}$, $\geq 10^{10.8}$, and $\geq 10^{11.3}$ cm^{-3} are found for the quiet Sun, active region, and the two flares, respectively. Observations of the F5 IV–V star Procyon, made with the *Extreme Ultraviolet Explorer* (*EUVE*) satellite, are compared and contrasted with the solar observations. It is confirmed that Procyon's average coronal conditions are very similar to those seen in the quiet Sun, with $N_e = 10^{9.4}$ cm^{-3}. In addition, although the quiet Sun is the closest solar analog to Procyon, we conclude that Procyon's coronal temperatures are slightly hotter than solar. A filling factor of 25^{+38}_{-12}% was derived for the corona of Procyon.

Subject headings: atomic data — line: identification — stars: individual (Procyon, α Canis Minoris) — Sun: corona — Sun: UV radiation

1. INTRODUCTION

In order to understand the nature of the physical processes that are responsible for heating the solar corona as well as the coronae of other stars, one must be able to accurately measure the physical properties of those environments. Emission lines in the extreme-ultraviolet (EUV) wavelength range (covering ~150–912 Å) are ideal for this purpose, coming from ions that form from $\sim 10^4$ to 10^7 K. One can use emission line ratios to derive electron temperatures (T_e) and/or densities (N_e), by comparison with the predictions of atomic model calculations incorporating accurate impact excitation rates and oscillator strengths (Mason & Bhatia 1978).

In this paper we focus on EUV emission lines from the sulphur-like ion Fe XI. This ion forms over the temperature range 6×10^5 to 3×10^6 K (which includes upper transition region through solar flare conditions), and is most abundant for $T_e = 10^{6.1}$ K (Brickhouse, Raymond, & Smith 1995). We analyze observations of both the solar corona and the corona of the nearby F5 IV–V star Procyon.

A number of other solar studies have previously been made that are relevant to our work. Kastner & Mason (1978) and Neupert & Kastner (1983) compared predicted line ratios to solar data from the Goddard *Orbiting Solar Observatories* (*OSO 7* and *OSO 5*). Brickhouse et al. (1995) also measured Fe XI line ratios in Solar EUV Rocket Telescope and Spectrograph (SERTS) spectra, and found an active-region density of $\log N_e \sim 10$. Brosius et al. (1996) derived coronal densities from Fe XIII lines in SERTS 91/93 data, and found $\log N_e = 9.6 \pm 0.5$ and 9.0 ± 0.3 for active region and quiet Sun, respectively. They also studied temperature-sensitive ratios, and found that the temperatures of these regions did not appear to be significantly different for the ions Fe X through Fe XIII. However, the active-region temperatures were seen to be higher for Fe XIV through Fe XVI, indicating that although the quiet-Sun and active-region temperature structures are very similar, the active regions do contain some hotter material. Brosius et al. (1997) compared SERTS-93 data with *Yohkoh* soft X-ray observations, and studied the hot loop structures seen in both X-rays and Fe XV–XVI. They found that active-region densities are ~2 times those in the quiet Sun. Brosius, Davila, & Thomas (1998a, 1998b) analyze SERTS-95 observations. They perform radiometric calibration using density- and temperature-insensitive line ratios, and present calibrated line lists for active-region and quiet-Sun areas. They also derive active-region densities from line ratios of Fe X through Fe XVI.

Coronal emission from cool stars such as Procyon has also been studied previously, using the *Extreme Ultraviolet*

[1] Now at Astrophysics Research Institute, Liverpool John Moores University, Twelve Quays House, Egerton Wharf, Birkenhead, CH41 1LD, UK; dpi@astro.livjm.ac.uk.

Explorer (*EUVE*) satellite. Brickhouse et al. (1995) measured Fe XI line ratios in Capella, but did not find consistent densities. Schrijver et al. (1995) analyzed the spectra of seven cool stars including Procyon, and used differential emission measure analysis to constrain their coronal temperature structure. They also used Fe X and Fe XII–Fe XIV lines to constrain the density of Procyon to 10^9–10^{10} cm^{-3}. Drake, Laming, & Widing (1995) presented a detailed study of element abundances in the corona of Procyon, and discussed the first ionization potential effect (or apparent lack of it). Schmitt et al. (1996) measured density-sensitive line ratios from Fe X–Fe XIV in Procyon, and derived a coronal density consistent with solar active regions. Schmitt, Haisch, & Drake (1994) and Laming (1998) also specifically analyze the coronal density of Procyon.

In this work, we have used the latest atomic physics calculations to derive both N_e-sensitive and N_e-insensitive theoretical Fe XI line ratios, which we compare to solar observations of the quiet Sun and an active region (taken from Brosius et al. 1998b), as well as to observations of two flares. We identify line blending in the spectra, and derive N_e values for each of the solar regions. We subsequently compared our theoretical ratios to observations of the nearby F5 IV–V star Procyon. By comparing and contrasting the stellar and solar observations, we identify line blends in Procyon's spectrum, and determine the average conditions in the corona of this star.

2. THEORETICAL LINE RATIOS

Collisional excitation data for Fe XI has previously been reported by Mason (1975), who used a distorted wave approximation to calculate collision rates at 8 ryd. Line strengths and ratios were subsequently derived by Kastner & Mason (1978), Neupert & Kastner (1983), and Brickhouse et al. (1995). More recently, collisional data have been presented by Bhatia & Doschek (1996), who derive collision strengths above the highest excitation threshold at 8, 16, and 24 ryd, but do not include resonance effects in their calculations. In this work, we use collisional data from Gupta & Tayal (1999a, 1999b; see also Tayal 2000, which presents similar calculations for lower T_e conditions). These calculations were made using a semirelativistic ***R***-matrix approach for the 20 *LS* states (38 fine-structure levels) considered. All the important electron correlation terms corresponding to the 3*d* and 4*f* orbitals were accounted for, and resulted in some large resonances for a few transitions. Energies and oscillator strengths for the model were taken from Deb & Tayal (1998). These atomic data were formatted appropriately for the CHIANTI atomic database (see Dere et al. 1997), and the CHIANTI software was used to calculate relative emission line strengths at the temperature of maximum ionization fraction (log $T_e = 6.1$), and as a function of electron density between 10^8 and 10^{12} cm^{-3}. The temperature dependence of collisional excitation was not significant for our derived ratios.

Table 1 lists the transitions responsible for the emission lines considered in this work, along with their wavelengths. Emission line ratios that we used are given in Table 2, where we have indicated the relevant emission lines by their wavelengths (taken from Table 1). In particular, R_1 through R_{11} are the N_e-sensitive ratios, while R_{12} through R_{18} are all very insensitive to N_e. We use the insensitive ratios to check for line blends (see § 4), and Table 2 also shows the relatively small range of theoretical values that these ratios have over the given N_e interval. We note that R_{16} and R_{17} have constant theoretical values, because they are branching ratios, where both the lines in each of them have common upper levels.

TABLE 1

WAVELENGTHS AND TRANSITIONS FOR THE EMISSION LINES CONSIDERED IN THE PRESENT WORK

Wavelength (Å)	Transition
178.06	$3s^2 3p^4\ ^3P_2 - 3s^2 3p^3(^4S)3d\ ^3D_2$
179.76	$3s^2 3p^4\ ^1D_2 - 3s^2 3p^3(^2D)3d\ ^1F_3$
180.41	$3s^2 3p^4\ ^3P_2 - 3s^2 3p^3(^4S)3d\ ^3D_3$
180.60	$3s^2 3p^4\ ^3P_1 - 3s^2 3p^3(^4S)3d\ ^3D_1$
181.14	$3s^2 3p^4\ ^3P_0 - 3s^2 3p^3(^4S)3d\ ^3D_1$
182.17	$3s^2 3p^4\ ^3P_1 - 3s^2 3p^3(^4S)3d\ ^3D_2$
184.41	$3s^2 3p^4\ ^1S_0 - 3s^2 3p^3(^2P)3d\ ^1P_1$
184.80	$3s^2 3p^4\ ^1D_2 - 3s^2 3p^3(^2D)3d\ ^1D_2$
188.23	$3s^2 3p^4\ ^3P_2 - 3s^2 3p^3(^2D)3d\ ^3P_2$
188.30	$3s^2 3p^4\ ^3P_2 - 3s^2 3p^3(^2D)3d\ ^1P_1$
189.13	$3s^2 3p^4\ ^3P_1 - 3s^2 3p^3(^2D)3d\ ^3P_1$
189.72	$3s^2 3p^4\ ^3P_0 - 3s^2 3p^3(^2D)3d\ ^3P_1$
192.83	$3s^2 3p^4\ ^3P_1 - 3s^2 3p^3(^2D)3d\ ^3P_2$
198.55	$3s^2 3p^4\ ^1D_2 - 3s^2 3p^3(^2D)3d\ ^3P_1$
202.71	$3s^2 3p^4\ ^1D_2 - 3s^2 3p^3(^2D)3d\ ^1P_1$

In Figure 1 we plot the N_e-sensitive ratios. As can be seen from the figure, R_1 and R_3 are the most N_e sensitive ratios, varying by factors of ~ 50 between $N_e = 10$ and 10^{12} cm^{-3}. By contrast, R_2 and R_7 vary by a factor of ~ 10 over the same density interval. Other ratios are not so N_e-sensitive, but all vary by factors of between 2.5 and 4 over the density range, and are thus all potentially useful for providing density diagnostics. A comparison with the predictions of CHIANTI version 2 (which contains the collisional data of Bhatia & Doschek 1996) shows general agreement at about the 20%–30% level from $N_e = 10^8$ to 10^{12} cm^{-3}. However,

TABLE 2

LINE RATIOS USED IN THIS WORK

Number	Line Ratio	*R* Range
	N_e-sensitive Line Ratios	
R_1	I(180.41 Å)/I(179.76 Å)	
R_2	I(181.14 Å)/I(179.76 Å)	
R_3	I(184.80 Å)/I(180.41 Å)	
R_4	I(180.41 Å)/I(182.17 Å)	
R_5	I(188.23 Å)/I(182.17 Å)	
R_6	I(192.83 Å)/I(182.17 Å)	
R_7	I(189.13 Å)/I(184.80 Å)	
R_8	I(184.80 Å)/I(189.72 Å)	
R_9	I(188.23 Å)/I(189.72 Å)	
R_{10}	I(181.14 Å)/I(192.83 Å)	
R_{11}	I(182.17 Å)/I(179.76 + 180.41 + 180.60 Å)	
	N_e-insensitive Line Ratios	
R_{12}	I(184.80 Å)/I(179.76 Å)	0.45–0.56
R_{13}	I(181.14 Å)/I(182.17 Å)	0.33–0.42
R_{14}	I(188.30 Å)/I(182.17 Å)	0.37–0.51
R_{15}	I(180.41 Å)/I(188.23 Å)	1.76–2.14
R_{16}	I(192.83 Å)/I(188.23 Å)	0.21
R_{17}	I(189.13 Å)/I(189.72 Å)	1.3
R_{18}	I(179.76 + 180.41 + 180.60 Å)/I(188.23 + 188.30 Å)	1.94–2.25

NOTE.—R_1–R_{11} are N_e-sensitive, while R_{12}–R_{18} are very insensitive to N_e. The theoretical values of the N_e-insensitive line ratios over the density interval $N_e = 10^8$–10^{12} cm^{-3} are also shown.

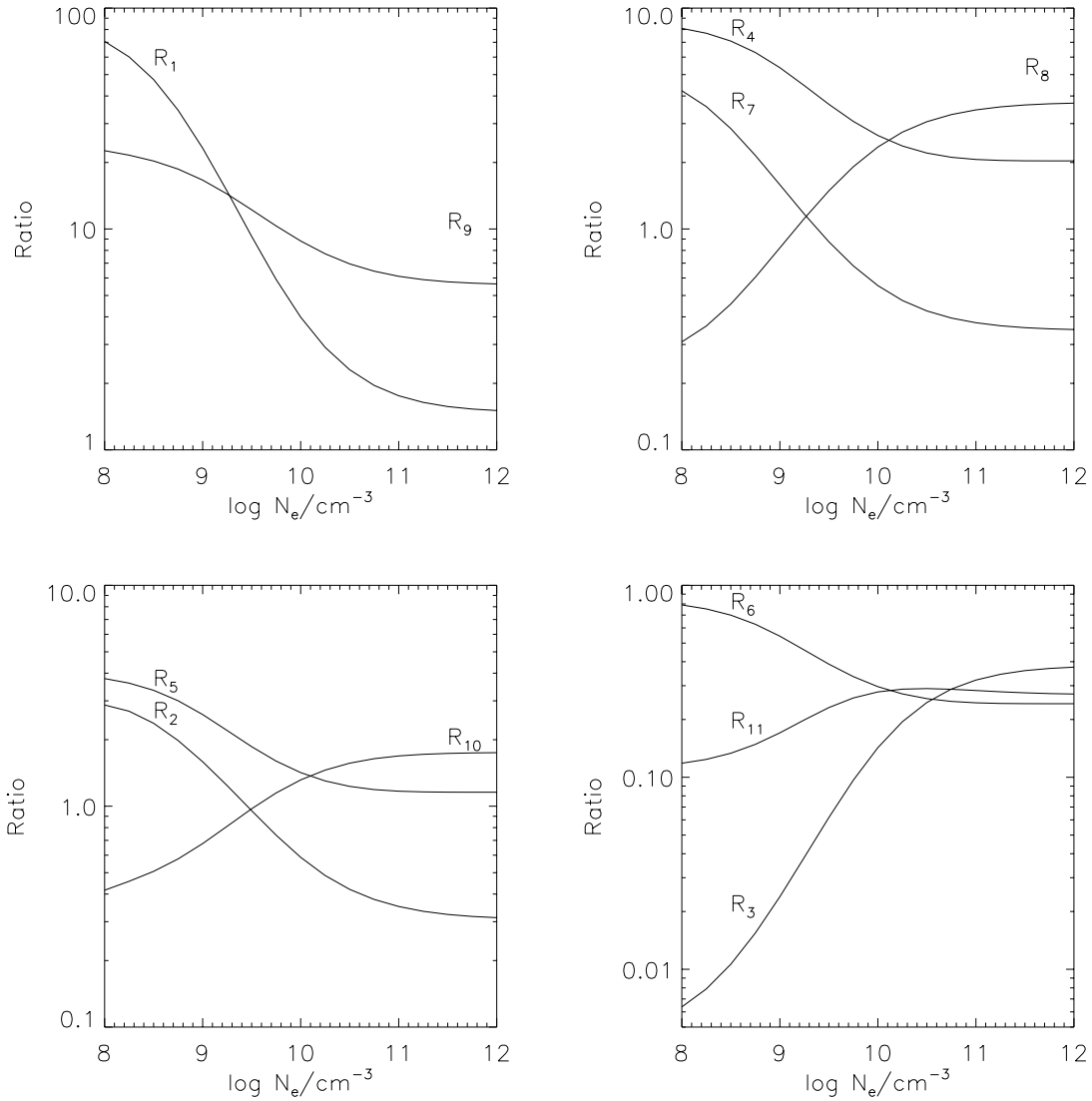

FIG. 1.—Theoretical density sensitive Fe XI emission line ratios R_1 to R_{11}, where the line strengths are in energy units, plotted as a function of log N_e (N_e in cm^{-3}), at the temperature of maximum Fe XI ionization fraction (log $T_e = 6.1$).

R_1, R_2, R_3, R_7, and R_9 differ by a factor of 2–3 for densities of $\sim 10^8$ cm^{-3}, where our ratios are lower except for R_3; R_3 is also $\sim 50\%$ higher at $\sim 10^{10}$ cm^{-3}. We note here that the factors of 2–3 do not affect the N_e values derived in this paper, since they are all between $\sim 10^9$ and 10^{11} cm^{-3}.

3. OBSERVATIONAL DATA

3.1. *SERTS-95 Observations*

The solar active region and quiet-Sun spectra considered in this work are for the region NOAA 7870 and quiet-Sun areas northeast of this. They were measured with the Solar EUV Rocket Telescope and Spectrograph, launched on 1995 May 15 (SERTS-95). This version of SERTS incorporated a multilayer coating that enhanced the sensitivity in the second order, and removed most of the first-order lines from the region of maximum second-order sensitivity ($\sim$185–205 Å). These observations were first presented in Brosius et al. (1998b), and a detailed description of the reduction process and line-extraction methods can be found therein. The quiet-Sun and active-region Fe XI lines that we consider here are all second-order lines in the range 178–203 Å, and are listed in Table 3.

3.2. *Skylab Observations*

Solar flare data were obtained by the Naval Research Laboratory Extreme Ultraviolet slitless spectroheliograph (5082A) aboard *Skylab*. The instrument employed a concave grating to photograph dispersed images of the Sun in the 171–630 Å wavelength range, with a spatial resolution of better than 3″, and spectral resolution of about 0.1 Å. Spectra were obtained by using a microdensitometer to trace along the dispersion axis at the desired spatial location. Our data comprise plate 3A-466, which was taken on 1974 January 21 at 2324 UT, and a scan through the hot *c*-kernel of this flare (see Widing & Hiei 1984 for a sketch of this location) from plate 3A-470 at 2346 UT. Flux calibration was performed using the data of Dere & Mango (1978), and line strengths are in general accurate to about $\pm 20\%$. The measured Fe XI lines are listed in Table 3.

3.3. *EUVE Observations*

We obtained a spectrum of Procyon taken by *EUVE*, which consists of a gold-plated grazing incidence telescope that focuses the flux into a slitless spectrograph consisting

TABLE 3

SOLAR EUV EMISSION LINES OF Fe XI

Wavelength (Å)	Quiet Sun	Active Region	1974 Jan 21 Flare, 2324 UT	1974 Jan 21 Flare, 2346 UT
178.06	...	...	...	...
179.76	...	...	9.7 ± 1.9	10.0 ± 2.0
180.41	528 ± 77	3440 ± 391[a]	13.0 ± 2.6	12.4 ± 2.5
180.60	...	...	...	...
181.14	...	123 ± 36[b]	3.4 ± 1.0	1.8 ± 1.2
182.17	121 ± 24	237 ± 33	...	...
184.41	...	...	4.2 ± 0.8[c]	...
184.80	...	32 ± 14	8.7 ± 1.7[d]	9.3 ± 1.9[d]
188.23	200 ± 46	385 ± 77	...	...
188.30	138 ± 34[e]	276 ± 52[e]	...	...
189.13	...	33 ± 9	...	...
189.72	...	26 ± 7	...	...
192.83	53 ± 14	68 ± 10	...	...
198.55	92 ± 22[f]	...	...	...
202.71	...	...	...	...

NOTE.—The quiet Sun and active region line strengths are in units of ergs cm^{-2} s^{-1} sr^{-1}, and the flare line strengths are in arbitrary units. Line blending is also summarized (see text for details).

[a] First-order Fe XVI blend at 360.4 Å.

[b] Low-level blend.

[c] Fe X + Ar XI blend.

[d] Ne V blend.

[e] Unknown blend.

[f] S VII blend.

of three gratings. Appropriate filters are also employed to isolate three spectral ranges, which are measured by microchannel plate detectors. The resulting bandpasses comprise the short-wavelength 70–190 Å, the medium-wavelength 140–380 Å, and the long-wavelength 280–760 Å regions, with a resolving power of $\lambda/\Delta\lambda \sim 200$. For more details see Welsh et al. (1990) and Bowyer & Malina (1991).

The *EUVE* observations were made from 1994 March 12 to 18, as part of an in-orbit calibration program. The total exposure time was 166 ks. Instrumental signatures were removed, and the intensity and wavelength calibration was performed using the IRAF-based EUV software EGOCS 1.6 and EGODATA 1.11 (Miller & Abbott 1995). The spectra were also corrected for interstellar extinction (see Foster et al. 1996). Line fluxes and central wavelengths were determined by fitting Gaussian profiles to the spectra using the STARLINK DIPSO routine.

4. RESULTS AND DISCUSSION

We adopted several approaches to identifying line blends in both the solar and the stellar observations. Initially, we used the density-insensitive ratios listed in Table 2 to show the presence of blended lines, by comparing the measured ratios with the theoretical values. We also used the CHIANTI *synthetic* routine to look for likely sources of any blending. This routine uses abundances from Allen (1973), ion equilibrium results from Arnaud & Rothenflug (1985), and distributed emission measures appropriate to whichever solar region is considered. Furthermore, we studied line profiles to look for any evidence of non-Gaussian shapes. A summary of the blends identified is given in Table 3 (see the following text for more details), along with the relative line strengths in each solar region. Values of N_e were then derived using lines that we had found to be not significantly blended (except for a fairly low level blend in one of the Procyon lines). Tables 5 and 6 give the resulting ratios and logarithmic electron densities (N_e in cm^{-3}) for each of the solar regions.

4.1. *Solar Spectra*

In the quiet Sun, the density-insensitive ratios R_{15} and R_{16} agree with theory, and we thus ruled out blends (to within the line flux errors) in the 180.41, 188.23, and 192.83 Å quiet-Sun lines. The R_{14} ratio is substantially higher than theory predicts, indicating that the 188.30 Å line is blended by $\sim$55%. However, there are no potential blends suggested by CHIANTI in second or first order. We also note that Brosius et al. (1998b) only tentatively associate this line with Fe XI. The 182.17 Å line should be unblended according to CHIANTI, and no evidence of blends is observed in the line profile. Using the four unblended lines, we derive N_e values using the density-sensitive ratios R_4, R_5, and R_6 (see Table 6), and all three ratios are consistent with a value of $\log N_e = 9.3$. This value agrees with the results of Brosius et al. (1996), who use the 308.5 Å/369.2 Å Fe XI line ratio to obtain $\log N_e = 9.37 \pm 0.31$. Employing Fe XIII line ratios, they also obtained $\log N_e$ values between 8.75 and 9.32. At lower ionization levels, Foster et al. (1996) and Young et al. (1996) found $\log N_e = 8.8^{+0.4}_{-0.7}$ and 9.3, respectively, from Fe X line ratios. We do not compare our densities with those found from Fe XII, since these yield systematically higher densities (see Brosius et al. 1996, 1998b). In addition, although there are no line ratios that are insensitive to density with which to test the 198.55 Å line, we note that the value of the I(198.55 Å)/I(182.17 Å) ratio is 0.76 ± 0.24, which is well above the predicted theoretical range of $\sim$0.1–0.2. This suggests a strong blend of at least 75%, where the likely source of this blend is S VII, as noted by Brosius et al. (1998b).

In the active region, the density-insensitive ratios R_{13}, R_{16}, and R_{17} agree with theory, and we thus rule out blends

(to within the errors) in the 181.14, 182.17, 188.23, 189.13, 189.72, and 192.83 Å lines. Once again however, the measured value of R_{14} is higher than theory predicts, indicating a blend in the 188.30 Å line to the same degree as in the quiet Sun. As discussed previously, there are some other misgivings about this line. CHIANTI indicates that the 180.41 Å line should be strongly blended with the Fe XVI resonance transition at 360.76 Å in first order, which was also noted by Brosius et al. (1998b). In addition, CHIANTI indicates that the 184.80 Å active-region line should be unblended, and we see no evidence of a blend in the line profile. We thus have seven essentially unblended lines, from which we derived N_e using the density-sensitive ratios R_5 through R_{10}. There is generally good agreement between these densities, where the estimates derived from the ratios R_5 through R_9 are all consistent with a value of $\log N_e = 9.7$. However, R_{10} gives a lower limit that is slightly higher than this value, but we note that we were only able to test the 181.14 Å line for blends at the $\sim 32\%$ level. A low-level blend at the $\sim 10\%$ level in this line would bring the R_{10} density into agreement with those from the other ratios, and we therefore assume that this is the most likely scenario. For comparison, Brosius et al. (1998b) used the same active-region data, and obtained densities of $\log N_e = 9.33^{+0.27}_{-0.41}$ and $9.54^{+0.21}_{-0.33}$ from the 184.80 Å/182.17 Å and 184.80 Å/188.23 Å Fe XI line ratios, respectively. These are consistent with the densities we find using R_5, R_7, R_8, and R_9. They are also reasonably consistent with the lower limit we find using R_6. However, we prefer our adopted $\log N_e$, since it is consistent with the higher values, as well as those centered around 9.4. Brosius et al. (1998b) also derived densities using a number of Fe X and Fe XIII line ratios, and found $\log N_e$ values grouped around either 9.2, 9.4, or 9.7. A more detailed treatment of line blending and updated atomic data may account for this spread, but our results lead us to prefer the higher value. We therefore find some evidence for a change in N_e of a factor of ~ 2.5 from the quiet Sun to the active region. This is similar to the factor of ~ 2 found by Brosius et al. (1997) for a different active region.

For the flare data, CHIANTI indicates that the 179.76, 180.41, and 181.14 Å lines should not be blended significantly. The 184.41 Å line should, however, be blended with the wing of Fe X emission at 184.54 Å, and also with Ar XI. This Fe X feature was detected in both the 1974 plates, but noise levels in the line wing mean that the 184.41 Å line was only detected in the 2324 UT observation. CHIANTI also indicates that the 184.80 Å flare line should be blended with Ne V emission at about the 30% level, and the density insensitive ratio R_{12} lends support to this assertion, since the ratios in both the 2324 and 2346 UT data are significantly higher than theory predicts, albeit with fairly large error bars. A blend of $\sim 40\%$ in this line seems likely. This blend is confirmed when we look at the value of R_3, since the ratio lies completely above the theoretical range, and the 184 Å flare line is thus not useful for density diagnostics. We have therefore used the 179.76, 180.41, and 181.14 Å lines to derive N_e values from R_1 and R_2 for the 2324 UT flare, and from R_1 for the 2346 UT flare since the 181.14 Å line strength suffers from 70% uncertainty in these data. The uncertainties associated with our ratios mean that we are only able to derive lower limits to the N_e values for the flares, and we find $\log N_e \geq 10.8$ and ≥ 10.3 from R_1 and R_2, respectively, in the 2324 UT data, and $\log N_e \geq 11.3$ for the 2346 UT spectrum. For comparison, Dere et al. (1979) measured Fe IX emission lines from this flare and found $\log N_e = 10.70 \pm 0.15$.

4.2. *Procyon Spectra*

We determined which lines contribute most significantly to Procyon's *EUVE* spectrum by comparing Procyon data with the quiet-Sun and the active-region spectra. We were then able to identify lines that could provide useful Fe XI density diagnostics.

Line blends in the Procyon spectrum are rather more involved than in the solar data, as a result of the lower spectral resolution. In order to determine which lines are the main contributors to the features observed in Procyon's spectrum, we convolved our solar active region and quiet-Sun spectra with the *EUVE* instrumental profile. The convolution was performed using the *specmod* IRAF routine within EGOCS. Figure 2 contains six plots, where the ordinates are in units of intensity, scaled for easy comparison. The top two plots contain the *EUVE* Procyon spectrum in the spectral region 178–195 Å. In the first of these, we have indicated the six spectral features that account for essentially all of Procyon's emission over this range. The features are at ~ 180, 182, 185, 187, 188, and 193 Å. The middle two plots contain the convolved SERTS-95 active-region and quiet-Sun spectra, respectively, and the bottom two plots are the original SERTS-95 spectra. We note that we have removed a strong feature from the quiet Sun at 182.3 Å, which we associate with a first-order line. The brighter emission lines in each region are labeled in the bottom two plots, and by examining their relative strengths, we can determine which are the main contributors to each of the features observed in the convolved spectra. These contributors are indicated in the middle two plots.

After comparing Procyon's spectrum to the convolved active-region spectrum, we note the following. First, there is a marked difference between the Procyon and active-region data at 180 Å, where this feature in the latter is much brighter with respect to other emission lines. Furthermore, the active-region features at 187 and 193 Å are brighter than those at 185 and 188 Å. These differences in the second-order spectrum can be explained by the presence of flux contributions from ions that are more highly ionized than Fe XI (such as Fe XVI at 180 Å in first order, and Fe XII at 187 and 193 Å), which are presumably more abundant in the active region. The active-region features at 182, 185, and 188 Å, which are dominated by flux from the less highly ionized ions Fe VIII, Fe X, and Fe XI, are detected at relatively weaker levels than in Procyon. These factors are all indicative of Procyon's corona having a lower T_e than the solar active region.

When we compared Procyon's spectrum to the convolved quiet-Sun data, however, we note a number of similarities. In particular, the relative heights of the 182, 184, 188, and 193 Å features are very similar. However, there is a slight difference at 180 Å, where this feature is relatively stronger in the quiet Sun. We attribute this difference to slightly higher levels of Fe XII emission in Procyon at 188 and 193 Å, which has increased the relative strength of these features. As a result, we conclude that the temperature of Procyon's corona is most similar to that of the quiet Sun (albeit slightly hotter), and we thus assume that the main flux contributors to the quiet-Sun spectrum are also responsible for Procyon's emission over this range. These

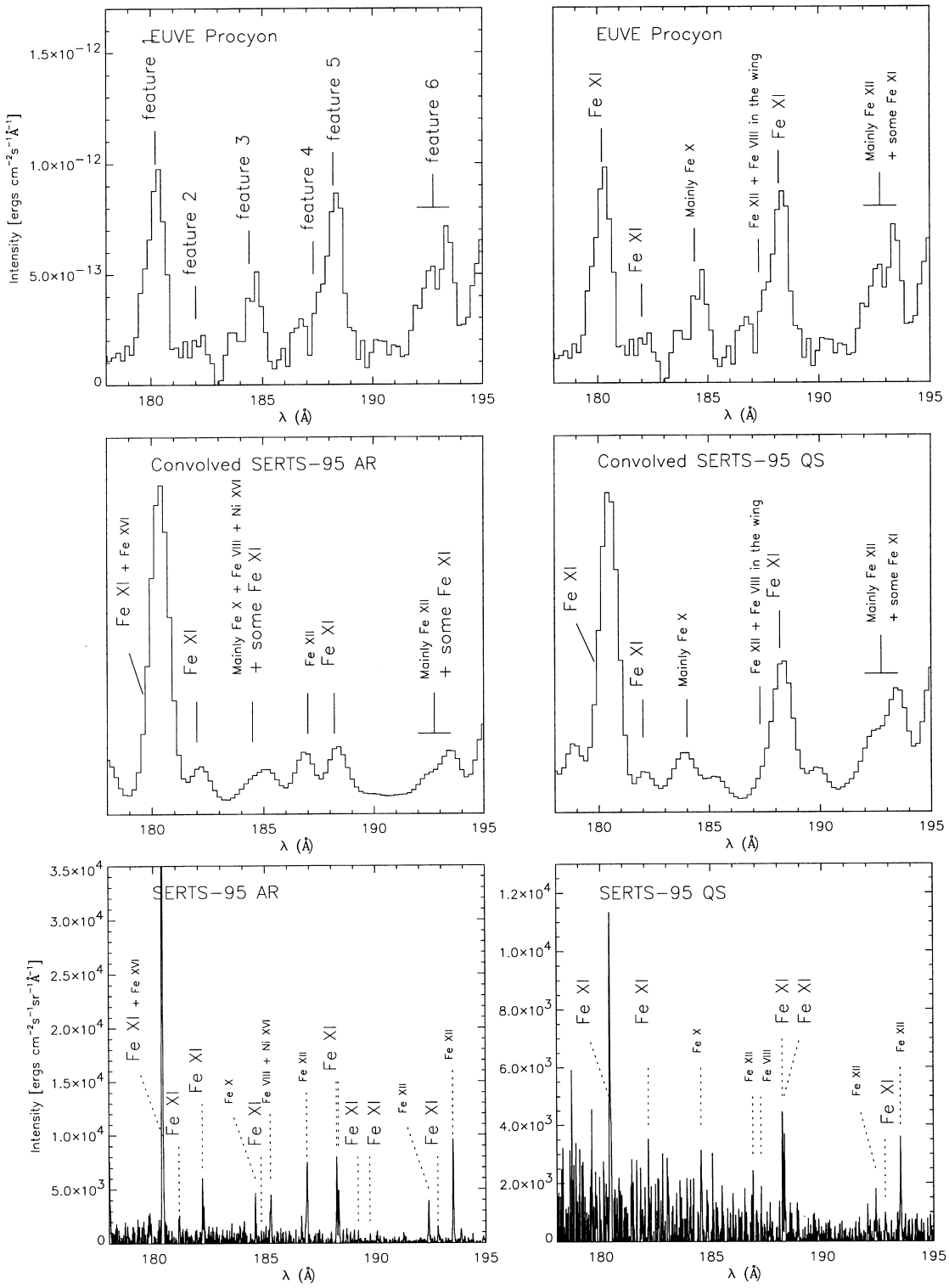

FIG. 2.—EUV spectra containing Fe XI emission lines. The top two plots are the *EUVE* Procyon spectrum. Spectral features are indicated in the first plot, and the main flux contributors in the second (see text). The signal-to-noise ratio of the data is ~15 in the peak of the brightest lines. The middle two plots contain the convolved SERTS-95 active-region (AR) and quiet-Sun (QS) spectra, respectively. The bottom two plots show the original SERTS-95 spectra, where we have removed a strong feature from the quiet Sun at 182.3 Å, which is a first-order line. The noise (3 σ) of the local background ranges from ~300 to 100 ergs cm^{-2} s^{-1} sr^{-1} Å^{-1} between 180 and 190 Å.

ions are indicated appropriately in the top right plot in Figure 2.

Table 4 summarizes the main emission-line contributors to the Procyon spectrum, and also gives the relative line strengths of each feature, found from our Gaussian fits. We fitted feature 6 with two Gaussians, where the blue component comprises Fe XII and Fe XI emission, and the red component is stronger Fe XII emission. By closely examining the relative strengths of these components in our spectra, we are able to make a more detailed comparison

TABLE 4

EMISSION STRENGTH IN PROCYON'S EUV SPECTRUM OVER THE WAVELENGTH RANGE 178–194 Å

Feature	Significant Contributors	Strength (10^{-12} ergs cm^{-2} s^{-1})
1 (180 Å).....	Fe XI (179.76 Å, low level)	10.93 ± 0.49
	(180.41 Å ~80%)	
	Fe X (180.41 Å ~20%)	
	Fe XI (180.60 Å, low level)	
	(181.14 Å, low level)	
2 (182 Å).....	Fe XI (182.17 Å dominates)	2.21 ± 0.44
3 (185 Å).....	Fe X (184.5 Å dominates)	6.13 ± 0.41
4 (187 Å).....	Fe XII (187.3 Å ~60%)	3.13 ± 0.59
	Fe VIII (186.9 Å ~40%)	
5 (188 Å).....	Fe XI (188.23 Å dominates)	7.10 ± 0.78
	(188.30 Å, low level)	
6 (193 Å).....	Fe XII (192.4 Å ~30%)	9.44 ± 0.33
	Fe XI (192.83 Å, low level)	
	Fe XII (193.5 Å dominates)	

NOTE.—Approximate wavelength is given in the first column. The emission lines primarily responsible for the flux in each feature are given in the second column, and the strength of each feature (from our Gaussian fits) is listed in the final column.

between the Procyon and solar spectra, to complement the visual comparison. The strength of the blue component in Procyon is ~70% that of the red component. This is very similar to the quiet-Sun feature, where the Fe XII and Fe XI line strengths total 78% that of the stronger Fe XII line. By comparison, for the active region feature, the blue component is only 56% as strong as the red one.

Regarding the Fe XI lines, we have three features that are potentially useful for providing N_e diagnostics, since the Fe XI line at 192 Å is swamped by Fe XII emission. These features are at 180, 182, and 188 Å. First, we consider the 180 Å feature. Schmitt et al. (1996) note that the Fe XI line at 180.41 Å is expected to be blended with an Fe X line at 180.41 Å. We have used the emission measure distribution of Procyon (Drake et al. 1995) and the line emissivities of Brickhouse et al. (1995) and estimate that the Fe X line contributes ~20% to the 180 Å feature. We next compare the density-insensitive ratio R_{18} to theory. The measured value of 1.54 ± 0.18 is slightly below the theoretical expectation, which is 1.94–2.25. Since we estimate that the 180 Å feature is blended by ~20%, the 188 Å feature must be blended by ~35%–45% to bring the measurement into agreement with the theoretically predicted range. It seems likely that the source of this blend is Fe XII and Fe VIII emission in the blue wing of the 188 Å feature, and that the uncertainties associated with our Gaussian fits to this particular line are slightly optimistic. We thus chose the 180 and 182 Å features, since we expect them to be dominated by Fe XI emission, and thus to be useful for density diagnostics. We used the density sensitive ratio R_{11} (see Table 5), and assumed a 20% blend in the 180 Å feature to obtain a value of $\log N_e = 9.40^{+0.30}_{-0.40}$ (see Table 6). This agrees with the results of Schmitt et al. (1996), who found $\log N_e = 9.20^{+0.80}_{-0.60}$ from this ratio. However, our density has a lower

TABLE 5

OBSERVED Fe XI LINE RATIOS FOR THE QUIET SUN (QS), ACTIVE REGION (AR), 1974 JANUARY 21 FLARE AT 2324 AND 2346 UT, AND PROCYON

Ratio	QS	AR	Flare 2324 UT	Flare 2346 UT	Procyon
R_1			1.35 ± 0.38	1.24 ± 0.25	
R_2			0.35 ± 0.13	0.18 ± 0.13	
R_3			0.67 ± 0.19	0.75 ± 0.21	
R_4	4.36 ± 1.09				
R_5	1.65 ± 0.50	1.61 ± 0.39			
R_6	0.44 ± 0.15	0.29 ± 0.06			
R_7		1.03 ± 0.53			
R_8		1.23 ± 0.48			
R_9		14.80 ± 5.03			
R_{10}		1.8 ± 0.59			
R_{11}					0.20 ± 0.04
R_{12}			0.90 ± 0.40	0.93 ± 0.40	
R_{13}		0.52 ± 0.17			
R_{14}	1.14 ± 0.36	1.16 ± 0.28			
R_{15}	2.64 ± 0.71				
R_{16}	0.27 ± 0.09	0.18 ± 0.05			
R_{17}		1.27 ± 0.48			
R_{18}					1.54 ± 0.18

TABLE 6

VALUES OF log N_e DERIVED FROM OUR LINE RATIOS MEASUREMENTS, FOR THE QUIET SUN (QS), ACTIVE REGION (AR), 1974 JANUARY 21 FLARE AT 2324 AND 2346 UT, AND PROCYON

	log N_e/cm^{-3}				
RATIO USED	QS	AR	Flare 2324 UT	Flare 2346 UT	Procyon
R_1			≥ 10.8	≥ 11.3	
R_2			≥ 10.3		
R_3			above theory	above theory	
R_4	9.30 ± 0.30				
R_5	9.70 ± 0.43	9.70 ± 0.35			
R_6	9.30 ± 0.5	≥ 9.70			
R_7		$9.37^{+0.76}_{-0.37}$			
R_8		$9.40^{+0.30}_{-0.40}$			
R_9		9.21 ± 0.57			
R_{10}		≥ 9.90			
R_{11}					$9.4^{+0.30}_{-0.40}$

uncertainty. Schmitt et al. also used the 182 Å/188 Å ratio to derive log $N_e = 8.15^{+0.85}_{-\infty}$, but as discussed above, we believe that the 188 Å feature is blended, which would have the effect of producing an erroneously low density. In addition, Schmitt et al. derived densities of log $N_e = 9.35^{+0.95}_{-0.45}$ and $9.20^{+0.20}_{-0.15}$ for Fe X and Fe XIII, respectively, while Foster et al. (1996) found log $N_e = 9.30 \pm 0.15$ from Fe X. All these values are in good agreement with our results. Our density is best represented by the quiet-Sun values. However, we note that it is also consistent with all but the lower limit (from R_{10}) of the active-region values.

We can use our derived density to estimate the filling factor f (the fraction of Procyon's corona that is actually responsible for the EUV emission). For this, we follow the approach taken by Schmitt et al. (1996), which involves equating the emission volume derived from the emission measure (EM/N_e^2) to the total visible coronal volume multiplied by f. We assume a magnetically confined corona, with a characteristic vertical height of $(\pi/4)L$, where L is the semilength of a typical coronal magnetic loop (see Rosner, Tucker, & Vaiana 1978). The loop scaling laws of Rosner et al. (1978) relate L to the temperature and density, where $N_e L = 1.3 \times 10^6 T_{\max}^2$ (where $T_{\max}$ is the loop apex temperature), and we thus substitute for L in our equality to derive f;

$$f = 1.56 \times 10^{-7} \frac{\mathrm{EM}}{N_e R^2 T_{\max}^2}, \quad (1)$$

where R is Procyon's radius (1.9 $R_\odot$), EM $= 4.5 \times 10^{50}$ cm^{-3} (Schmitt et al. 1996), and $T_{\max} = 2.5 \times 10^6$ K, the temperature observed in solar magnetic loops (Rosner et al. 1978). Our best-fit N_e value of 2.5×10^9 cm^{-3} gives a filling factor of 25%, and taking the uncertainty into account has a range of 13%–63%. This represents an improvement on the value found by Schmitt et al. (1996), who could not rule out a filling factor of 1.0, as a result of the uncertainties in their derived density (found using the same ratio as we used). However, we acknowledge that, as with the Schmitt et al. result, the major source of uncertainty is ambiguities in the choice of $T_{\max}$, which increases the range of possible f values.

In conclusion, we have confirmed that the conditions in Procyon's corona are very similar to those observed in the quiet Sun, with densities that are the same to within our measured uncertainty. We further conclude from our discussion that Procyon's average coronal T_e is slightly higher than that in the quiet Sun, but is closer to this temperature than that of any other solar region. It is therefore clear that detailed high-resolution studies of EUV emission lines from the quiet Sun can be used to provide an excellent analogy to those from the corona of Procyon and similar stars. Such solar observations will thus allow us to accurately deblend many features detected in the spectra of such stars, where a reduced signal-to-noise ratio precludes higher resolution observations. We will subsequently be able to accurately measure the stellar coronal properties.

D. J. P. acknowledges funding from the Leverhulme Trust. The SERTS rocket program is funded under NASA RTOP 344-17-38. The work of K. W. was supported in part by the ONR/NRL Research Option Solar Magnetism and the Earth's Environment.

REFERENCES

Allen, C. W. 1973, Astrophysical Quantities (London: Athlone)
Arnaud, M., & Rothenflug, R. 1985, A&AS, 60, 425
Bhatia, A. K., & Doscheck, G. A. 1996, At. Data Nucl. Data Tables, 64, 183
Bowyer, S., & Malina, R. F. 1991, in Extreme Ultraviolet Astronomy, ed. R. F. Malina & S. C. Bowyer (Elmsford, NY: Pergamon), 397
Brickhouse, N. S., Raymond, J. C., & Smith, B. W. 1995, ApJS, 97, 551
Brosius, J. W., Davila, J. M., & Thomas, R. J. 1998a, ApJ, 497, L113
———. 1998b, ApJS, 119, 255
Brosius, J. W., Davila, J. M., Thomas, R. J., & Monsignori-Fossi, B. C. 1996, ApJS, 106, 143
Brosius, J. W., Davila, J. M., Thomas, R. J., Saba, J. L. R., Hara, H., & Monsignori-Fossi, B. C. 1997, ApJ, 477, 969
Deb, N. C., & Tayal, S. S. 1998, At. Data Nucl. Data Tables, 69, 161
Dere, K. P., Landi, E., Mason, H. E., Monsignori Fossi, B. C., & Young, P. R. 1997, A&AS, 125, 149
Dere, K. P., & Mango, S. A. 1978, NRL Internal Rept.
Dere, K. P., Mason, H. E., Widing, K. G., & Bhatia, A. K. 1979, ApJS, 40, 341
Drake, J. J., Laming, J. M., & Widing, K. G. 1995, ApJ, 443, 393
Foster, V. J., Mathioudakis, M., Keenan, F. P., Drake, J. J., & Widing, K. G. 1996, ApJ, 473, 560
Gupta, G. P., & Tayal, S. S. 1999a, ApJ, 510, 1078
———. 1999b, ApJS, 123, 295
Kastner, S. O., & Mason, H. E. 1978, A&A, 67, 119
Laming, J. M. 1998, in ASP Conf. Ser. 154, Tenth Cambridge Workshop on Cool Stars, Stellar Systems, and the Sun, ed. R. A. Donahue & J. A. Bookbinder (San Francisco: ASP), 447
Mason, H. E. 1975, MNRAS, 170, 651
Mason, H. E., & Bhatia, A. K. 1978, MNRAS, 184, 423
Miller, A., & Abbott, M. 1995, *EUVE* Guest Observer Software, Version 1.5 (Berkley: CfA)
Neupert, W. M., & Kastner, S. O. 1983, A&A, 128, 181

Rosner, R., Tucker, W. H., & Vaiana, G. S. 1978, ApJ, 220, 643
Schmitt, J. H. M. M., Drake, J. J., Haisch, B. M., & Stern, R. A. 1996, ApJ, 467, 841
Schmitt, J. H. M. M., Haisch, B. M., & Drake, J. J. 1994, Science, 265, 1420
Schrijver, C. J., Mewe, R., van den Oord, G. H. J., & Kaastra, J. S. 1995, A&A, 302, 438
Tayal, S. S. 2000, ApJ, 544, 575
Welsh, B. Y., Vallerga, J. V., Jelinsky, P., Vedder, P. W., Bowyer, S., & Malina, R. F. 1990, Opt. Eng., 29, 752
Widing, K., & Hiei, E. 1984, ApJ, 281, 426
Young, P. R., Mason, H. E., Bhatia, A. K., Doschek, G. A., & Thomas, R. J. 1996, in IAU Symp. 152, Astrophysics in the Extreme Ultraviolet (Dordrecht: Kluwer), 583